Journal of Alloys and Compounds. Vol. 431. Núm. 1-2. 2007. Pag. 100-106
http://dx.doi.org/10.1016/j.jallcom.2006.05.054

Thermal and microstructural dependence of the initial permeability of $Co_{60}Fe_{18}Nb_6(B,Cu)_{16}$ alloys

J.S. Blázquez[1], V. Franco[1], C.F. Conde[1], A. Conde[1] and L.F. Kiss[2]

[1]Dpto. Física de la Materia Condensada, ICMSE-CSIC, Universidad de Sevilla, P. O. Box 1065, 41080, Sevilla, Spain;

[2]Research Institute for Solid State Physics and Optics, Hungarian Academy of Sciences, P. O. Box 49, 1525, Budapest, Hungary

Abstract. The thermal and microstructural dependence of the initial permeability of $Co_{60}Fe_{18}Nb_6B_{16-y}Cu_y$ (y=0, 1) alloys have been studied. The comparison of kinetics and microstructural data of the two compositions indicate the existence of a Cu-clustering phenomenon prior to the nanocrystallization for the alloy with Cu. These data are correlated with the evolution of the permeability as the devitrification progresses. From the technological point of view, samples treated up to the final stages of nanocrystallization exhibit temperature coefficients of the initial permeability one order of magnitude better than those of conventional nanocrystalline alloys or Mn-ferrites and a maximum temperature of applicability ~300 K higher.

Keywords: A-amorphous materials, A-high temperature alloys, A-nanostructured materials, C-microstructure, D-magnetic measurements.

*Corresponding author: A. Conde

Departamento de Física de la Materia Condensada. Universidad de Sevilla.

Apartado 1065, 41080 Sevilla (Spain).

Phone: (34) 95 455 28 85

Fax: (34) 95 461 20 97

E-mail: conde@us.es

Journal of Alloys and Compounds. Vol. 431. Núm. 1-2. 2007. Pag. 100-106
http://dx.doi.org/10.1016/j.jallcom.2006.05.054

1 Introduction

Fe-based nanocrystalline alloys, in which Fe-rich crystallites of about 10 nm are embedded in a residual amorphous matrix, have been developed as excellent candidates for soft magnetic applications (see for example Ref. [1] and references therein). However, these applications are limited to temperatures at which the nanocrystals are magnetically coupled yielding an averaging out of the magnetocrystalline anisotropy [2]. This requirement is not fulfilled at temperatures above the Curie temperature of the amorphous phase, T_C^{am}. In the so-called HITPERM alloys, the partial substitution of Co for Fe extends the applicability of nanocrystalline alloys up to higher temperatures, due to the increase of the Curie temperature of the residual amorphous phase [3]. However, the presence of Co in the crystalline phase increases its magnetostriction with respect to the Co-free α-Fe phase (~60 ppm and -9 ppm, respectively), leading to a deterioration of the room temperature soft magnetic character of the material at room temperature with respect to conventional nanocrystalline compositions [4]. For certain high temperature technological applications (e.g. LC filters), the requirement of a broad temperature range in which the magnetic properties are constant enough could be more desirable than just the achievement of better soft magnetic properties but with a stronger thermal dependency. In this sense, although FINEMET [5] and NANOPERM [6] alloys are magnetically softer, HITPERM alloys exhibit a less pronounced thermal dependency of coercivity [7], magnetization [3] and initial magnetic permeability (μ) [8], favoring their applicability at high temperatures.

In this work, the devitrification transformation of two HITPERM type alloys with high Co content is studied in detail in order to understand the thermal and microstructural dependence of the initial permeability. The two compositions, $Co_{60}Fe_{18}Nb_6B_{16-x}Cu_x$ (x = 0, 1), were chosen to clarify the effect of Cu addition on these

alloys. A previous study [9] was devoted to describe the relationship between room temperature coercivity and microstructure in the alloy series $Co_{78-y}Fe_yNb_6B_{16-x}Cu_x$ (y = 18, 39, 60; x = 0, 1).

2. Experimental

Ribbons (~ 5 mm wide and ~ 25 μm thick) of $Co_{60}Fe_{18}Nb_6B_{16-x}Cu_x$ (x = 0, 1) compositions were prepared by the single roller melt-spinning technique. The initial permeability measurements were performed during *in situ* continuous heating-cooling cycles. Toroidal samples were measured at a frequency of 6 kHz and an applied field of ~ 0.5 A/m, low enough to assure the measurement of initial permeability. Two coils were wounded around the sample. An ac field is applied with the first coil and the signal induced in the second coil is detected using a lock-in technique. An impedance analyzer (Hewlett-Packard 4192A) was used to calibrate the values of permeability at room temperature. The devitrification process of as-cast samples was characterized by differential scanning calorimetry (DSC) in a Perkin-Elmer DSC-7 at the same heating rate as that of the permeability measurements (5 K/min). Thermomagnetic gravimetry (TMG) performed in a Perkin-Elmer TGA-7, applying to the sample the magnetic field of a small magnet (~20 mT), was used for a complementary characterization of the magnetic transitions. Microstructure of samples at the last stages of nanocrystallization (heated up to 823 K) was characterized by X-ray diffraction (XRD) with Cu-Kα radiation and the evolution of the grain size as the nanocrystallization progresses was studied on samples annealed for different times at 55 K below the peak temperature of the nanocrystallization exotherm by transmission electron microscopy (TEM) in a Philips CM20 operated at 200 kV. The annealing temperature was achieved by using a three ramps heating procedure (~6 min) in order to avoid overshooting.

Journal of Alloys and Compounds. Vol. 431. Núm. 1-2. 2007. Pag. 100-106
http://dx.doi.org/10.1016/j.jallcom.2006.05.054

3. Results and discussion

3.1 Devitrification process

Figure 1 shows the DSC scan as well as the thermal dependence of the initial permeability, at a heating rate of 5 K/min, for as-cast samples of the two studied alloys. A correlation can be observed between both plots, which will be studied in detail below.

DSC plots show two main transformation stages, although using a lower heating rate (2.5 K/min) a third peak is observed below 1000 K for both alloys [10]. The thermally activated character of the process shifts this third exotherm to temperatures above the explored range for a heating rate of 5 K/min. A nanocrystalline microstructure formed by α-Fe(Co) crystallites embedded in a residual amorphous matrix is developed during the first transformation stage. For both alloys, the first DSC exotherm is broad (~100 K wide) and asymmetric unlike the second transformation stage, which is sharper (~50K wide) and symmetric. It can be observed that Cu addition decreases the onset temperature of the first transformation stage, which could be ascribed to the Cu-clustering phenomenon previous to the onset of nanocrystallization, which would enhance the nucleation of the α-Fe(Co) phase. In fact, although Cu rich clusters were detected for $Fe_{39}Co_{39}Nb_6B_{15}Cu_1$ alloy [11], Cu-clustering does not occur for Zr-containing HITPERM alloys [12] and a decrease of the number density of these clusters has been reported for Co-containing FINEMET alloys as the Co content increases [13]. However, for the studied alloys, the Cu addition does not only decrease the onset temperature of the first transformation stage, but it can also be observed that the shape of the nanocrystallization peak is clearly affected. From the DSC scans obtained at 5 K/min and the values of the activation energy (Q=3.5 and 3.1 eV for Cu-free and Cu-added alloys, respectively [10]) it is possible to extract some information about the

transformation kinetics of the system, using a procedure detailed elsewhere [14]. Figure 2 shows the local Avrami exponent as a function of the transformation fraction. Lower values of the local Avrami exponent can be found for the alloy with Cu with respect to the alloy without Cu (~0.7 and ~0.9, respectively) at the early stages of nanocrystallization, although they converge to a common value of ~0.3 at the end of the nanocrystallization process. This fact indicates that some differences exist in the nanocrystallization kinetics at the early stage of the process between the two studied alloys, which can be correlated with the Cu-clustering phenomenon.

3.2 Microstructural characterization

Figure 3 shows the XRD pattern for samples heated up to the end of the first stage of transformation (823 K). The amorphous halo and broad crystalline peaks corresponding to the α-Fe(Co) type phase can be observed. Neither hexagonal nor fcc Co-type phases have been detected. These phases would be expected for a Co content of the nanocrystals higher than 77 at. % [15]. In the studied cases, the Co-partitioning during the nanocrystallization was measured by 3D-atom probe technique and the concentration of Co was almost constant throughout the amorphous matrix and the nanocrystals, ~60 at. % of Co, independently of the crystalline volume fraction [11]. Therefore, the nanocrystals are strongly enriched in Fe with respect to the residual amorphous matrix. The impoverishment in Fe of the residual amorphous matrix would be the reason of the low crystalline volume fractions achieved at the end of the nanocrystallization ~40 % [16].

TEM images show a similar nanocrystalline microstructure for both studied alloys. Figure 4 shows bright field images of samples annealed during 60 and 750 min at 669 and 686 K, respectively for the alloys with Cu and without Cu (~55 K below the

corresponding DSC peak temperature). Figure 5 shows the grain size distributions obtained for samples annealed at these temperatures during different times. As can be observed, grain size distributions become similar for both alloys at long time of annealing but, at the early nanocrystallization stages, the alloy without Cu shows a slightly broader distribution. Figure 6 shows the average value of the grain size, <D>, and the total crystalline volume, V_{TEM}, measured as $\sum D_i^3$ over TEM dark field images. Dark field mode was used in order to obtain a better resolution of the individual nanocrystals. It is worth noting that V_{TEM} is meaningless unless it is derived from at least two dark field images (the crystallites which are not properly oriented will not be counted) obtained in the same conditions (same magnification and a constant value of the explored volume of the sample). In such a case, V_{TEM} must be proportional to the crystalline volume fraction. Under these considerations, the alloy without Cu shows slightly higher values of <D> and V_{TEM}. The small difference in <D> at the early stages of nanocrystallization (isothermal annealing) between the alloys with and without Cu remains between each couple of samples of the two compositions submitted to equivalent annealing procedures. Although for each individual datum an error bar ~ 1 nm must be considered, the global comparison between all the set of data suggests that a real small difference exists. As the isothermal annealing below the nanocrystallization onset temperature does not complete the nanocrystallization process even for very long annealing times [17], these results could not be ascribed to the final stages of nanocrystallization. They indicate that the crystallization is faster for Cu-free alloy than for the alloy with Cu, in agreement with a higher value of the Avrami exponent at the early stages of transformation, described in the previous section.

3.3 Initial permeability

Journal of Alloys and Compounds. Vol. 431. Núm. 1-2. 2007. Pag. 100-106
http://dx.doi.org/10.1016/j.jallcom.2006.05.054

The μ plots shown in figure 1 were obtained extracting the data from a continuous heating and cooling experiment, using only the values of μ obtained at temperatures above the maximum achieved temperature in the previous treatment. Two main events can be observed in this curve: a characteristic Hopkinson peak and a strong fall in permeability at higher temperatures, ~900 K. The coincidence in temperature of the latter and the second crystallization stage detected by DSC can be clearly observed in Fig. 1. This stage includes a partial recrystallization phenomenon involving part of the α-Fe(Co) nanocrystals developed during the first transformation stage and the residual amorphous matrix. The formation of these new phases destroys the nanocrystalline microstructure and yields a strong magnetic hardening of the material [18].

The Hopkinson peak occurs due to a faster decrease to zero of the magnetization than that of the magnetic anisotropy as the temperature increases, and thus the permeability diverges at the Curie point [19]. Figure 7 shows the TMG plots for as-cast samples of the two studied alloys. The fall of the magnetization at the Curie temperature of the amorphous alloys overlaps with an increasing contribution due to the nanocrystallization progress, even using the maximum heating rate allowed in the equipment (200 K/min). The temperature of the local minimum of magnetization, T_K, from TMG plots (see Fig. 7) is always higher than the temperature value of the corresponding Hopkinson peak maximum. The T_K value corresponds to the temperature at which the tendency to fall of the magnetization due to the proximity of the Curie temperature is overcome by the tendency to rise of the magnetization due to the formation of the ferromagnetic α-Fe(Co) phase. Therefore, $T_K \leq T_C^{am}$ and, it must be concluded that, for the studied alloys, the Hopkinson peak seems to occur below the Curie point of the amorphous matrix. This can be explained as an effect of the formation

of α-Fe(Co) nanocrystals with a higher Curie temperature. As the amount of crystalline phase increases, neither the magnetization nor the magnetic anisotropy decrease to zero but to a finite value (that of the crystalline phase) and thus the Hopkinson peak must be gradually smeared out as the crystalline volume fraction increases. This is in agreement with the overlapping between the onset of nanocrystallization (DSC plot) and the Hopkinson peak observed in figure 1. This overlapping is stronger in the case of the alloy with Cu with respect to the Cu-free alloy, which is in agreement with a lower value of the maximum permeability at the Hopkinson peak for the former alloy. The faster kinetics of the Cu-free alloy at the early stages of nanocrystallization with respect to the alloy with Cu can be correlated with the more abrupt fall of the permeability after the Hopkinson peak, with a slope of ~17 K^{-1}, observed for the Cu-free alloy than that observed for the alloy with Cu (~8.5 K^{-1}).

Figure 8 shows the initial permeability measured during continuous heating at 5 K/min for samples previously heated at different temperatures. For each alloy, the highest temperature label is marked with an asterisk, indicating that the curve was obtained during cooling down the samples (~5 K/min) from this temperature (maximum achieved temperature during the whole experiment). In order to clarify the figure, plots for amorphous samples have been separated from those of nanocrystalline samples. Generally, the curves can be considered reversible up to the temperature at which the sample was previously heated, although, in some cases, transformation continues during subsequent cooling due to thermal inertia. Figure 9 shows the main parameters obtained from plots of figure 8: initial permeability at 400 K, maximum temperature at which the curve can be considered reversible, T_{MAX}^{REV}, and the temperature coefficient of the initial permeability, defined as the relative change in μ from 400 K up to T_{MAX}^{REV} divided by the temperature span ($T_{MAX}^{REV} - 400$ K).

Journal of Alloys and Compounds. Vol. 431. Núm. 1-2. 2007. Pag. 100-106
http://dx.doi.org/10.1016/j.jallcom.2006.05.054

For amorphous samples, it can be observed that the initial permeability at a constant temperature increases as the temperature of the previous treatment increases, due to the release of internal stresses. It is worthy to note that annealing below T_C^{am} but applying an ac magnetic field avoids the domain wall pinning phenomenon, which would produce a moderate magnetic hardening of the material [20]. As it was said above, the maximum of the Hopkinson peak appears at (or slightly above) the crystallization onset, so it might be considered in the irreversible part of the curves.

For nanocrystalline samples with low crystalline volume fraction, the Hopkinson peak can be still identified, although it is strongly reduced and smeared. The permeability values are comparable to those of the amorphous samples (~10^3) but the temperature coefficient in the reversible temperature range shows smaller values. As the nanocrystallization progresses the initial permeability at 400 K decreases, the temperature coefficient generally decreases but T_{MAX}^{REV} is continuously enhanced. For samples at the final stages of nanocrystallization, the alloys show an increase of the permeability at high temperature, more noticeable for the alloy with Cu, in agreement with the slower kinetics of the transformation for this alloy with respect to the Cu-free alloy, for which, during the early stages of the process, the transformation is more developed.

Finally, above the second transformation stage observed by DSC, although the temperature range of stability increases, both the permeability and the temperature coefficient are worse than the values observed for nanocrystalline samples. The formation of borides which are hard magnetic phases with respect to α-Fe(Co) is the responsible for the deterioration of the soft magnetic character of the system.

The relevance of the technological application (for example as LC filters) can be evaluated after a comparison of the optimum values (observed for nanocrystalline

samples with relatively high crystalline volume fraction) obtained in the studied case with respect to those of other typical materials. For example, Mn ferrites show typical values of the temperature coefficient of ~0.3 %/K and they are limited to low temperatures (~500 K) due to their low Curie temperature [21]. Conventional nanocrystalline alloys, as FINEMET, exhibit much higher permeability although similar values of the temperature coefficient than those of Mn ferrites in a similar temperature range [22, 23]. The authors reported similar HITPERM-type compositions with lower Co content to have 0.02 %/K up to 900 K [8]. In the studied case, the temperature coefficient can be reduced a half (~ 0.01 %/K for both Cu-free and Cu-added alloys) but the permeability is only ~75 % of that of $Fe_{39}Co_{39}Nb_6B_{15}Cu_1$ alloy and the maximum temperature is 750 K.

Conclusions

The dependence of the initial permeability on the microstructure of $Co_{60}Fe_{18}Nb_6B_{16-y}Cu_y$ (y=0, 1) alloys has been studied. Kinetics and microstructural data were correlated with the evolution of the initial permeability as the crystallization transformation progresses.

From the technological point of view, samples treated up to the final stages of nanocrystallization exhibit temperature coefficients of the initial permeability an order of magnitude lower than that of conventional nanocrystalline alloys or Mn-ferrites and a maximum temperature of applicability ~300 K higher.

Acknowledgements

This work was supported by the Spanish Government and EU-FEDER (Project MAT 2004-04618), the PAI of Junta de Andalucía and the Hispano-Hungarian Bilateral

Cooperation Program (HH2004-0015, E-21/04). J. S. Blázquez is grateful to Junta de Andalucía for a research contract.

References

[1] M. E. McHenry, M. A. Willard, D. E. Laughlin, Prog. Mater. Sci. 44 (1999) 291.

[2] A. Hernando, M. Vázquez, T. Kulik, C. Prados, Phys. Rev. B 51 (1995) 3581.

[3] M. A. Willard, D. E. Laughlin, M. E. McHenry, D. Thoma, K. Sickafus, J. O. Cross, V. G. Harris, J. Appl. Phys. 84 (1998) 6773.

[4] O'Handley RC. Modern Magnetic Materials: Principles and Applications. New York: Wiley, 1999. p. 227.

[5] Y. Yoshizawa, S. Oguma, K. Yamauchi, J. Appl. Phys. 64 (1988) 6044.

[6] K. Suzuki, A. Makino, N. Kataoka, A. Inoue, T. Masumoto, Mater. Trans. JIM 32 (1991) 93.

[7] I. Skorvanek, P. Svec, J. Marcin, J. Kovac, T. Krenicky, M. Deanko, Phys. Stat. Sol. (a) 196 (2003) 217.

[8] J. S. Blázquez, V. Franco, A. Conde, L. F. Kiss. J. Appl. Phys. 93 (2003) 2172.

[9] J. S. Blázquez, V. Franco, A. Conde, J. Phys.: Cond. Matter 14 (2002) 11717-11727.

[10] J. S. Blázquez, C. F. Conde, A. Conde, J. Non-Cryst. Solids 287 (2001) 187.

[11] Y. Zhang, J. S. Blázquez, A. Conde, P. J. Warren, A. Cerezo. Mater Sci. Eng. A 353 (2003) 158.

[12] D. H. Ping, Y. Q. Wu, K. Hono, M. A. Willard, M. E. McHenry, D. E. Laughlin. Scripta Mater. 45 (2001) 781.

[13] M. Ohnuma, D. H. Ping, T. Abe, H. Onodera, K. Hono, Y. Yoshizawa, J. Appl. Phys. 93 (2003) 9186.

[14] J. S. Blázquez, C. F. Conde, A. Conde, Acta Mater. 53 (2005) 2305.

[15] T. B. Massalski, H. Okamoto, P. R. Subramanian, L. Kacprzak. Binary Alloys Phase Diagrams. Materials Park, Ohio: ASM International, 1992.

[16] J. S. Blázquez, V. Franco, C. F. Conde, A. Conde, J. Magn. Magn. Mat. 254 (2003) 460.

[17] C. F. Conde, A. Conde, Mater. Sci. Forum 179-181 (1995) 581.

[18] J. S. Blázquez, C. F. Conde, A. Conde, Appl. Phys. Letters 79 (2001) 2898.

[19] M. Kersten, Z. Angew. Phys. 8 (1956) 313.

[20] V. V. Shulika, A. P. Potapov, J. Phys. IV 8 (1998) Pr2-147

[21] A. A. Saltar, J. Mater. Sci. 39 (2004) 451.

[22] V. Franco, C. F. Conde, A. Conde, L. F. Kiss, J. Magn. Magn. Mater. 215-216 (2000) 400.

[23] Z. Wang, K. He, J. Jin, J. He, L. Zhang, H. Zhang, B. Shen, Mater. Sci. Eng. A 304-306 (2001) 1046.

Journal of Alloys and Compounds. Vol. 431. Núm. 1-2. 2007. Pag. 100-106
http://dx.doi.org/10.1016/j.jallcom.2006.05.054

Figure Captions

Figure 1. DSC plots for as cast samples and initial permeability values (see text) as a function of temperature (heating rate of 5 K/min) for the two studied alloys.

Figure 2. Local Avrami exponent as a function of the total enthalpy fraction involved in the nanocrystallization process (from DSC) for the two studied alloys.

Figure 3. XRD patterns of nanocrystalline samples of the two studied alloys (heated up to 823 K).

Figure 4. Bright field images and selected area diffraction patterns of samples annealed 60 and 750 min at 55 K below the peak temperature of the nanocrystallization process of each alloy.

Figure 5. Grain size distribution of samples annealed during different times at 55 K below the peak temperature of the nanocrystallization process.

Figure 6. Average grain size (<D>) and total crystalline volume measured on a dark field image (ΣD_i^3) as a function of the annealing time at 55 K below the peak temperature of the nanocrystallization process. Lines are drawn as a guide to the eye.

Figure 7. TMG plots of as cast samples of the two studied alloys. T_K indicates the temperature at which the local minimum of the magnetization occurs.

Figure 8. Temperature dependence of the initial permeability for samples heated up to different temperatures indicated by labels. Symbols do not correspond to individual data and are plotted to facilitate the identification of the curves. Curves marked with an asterisk (fully crystallized samples) were recorded during cooling.

Figure 9. Permeability value at 400 K, maximum temperature at which each curve of Fig. 8 is reversible and temperature coefficient of μ between 400 K and this temperature for different annealed samples of the two studied alloys. Lines are drawn as a guide to the eye.

Journal of Alloys and Compounds. Vol. 431. Núm. 1-2. 2007. Pag. 100-106
http://dx.doi.org/10.1016/j.jallcom.2006.05.054

Figure 1

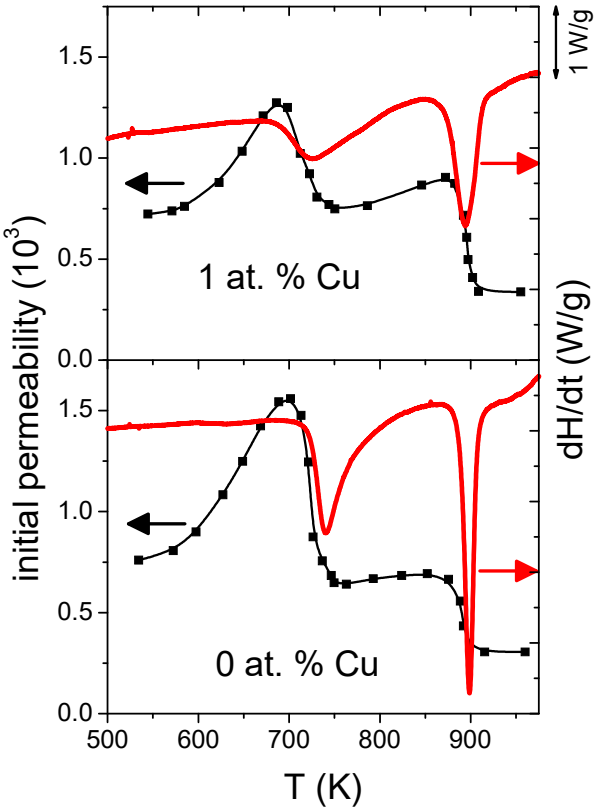

Journal of Alloys and Compounds. Vol. 431. Núm. 1-2. 2007. Pag. 100-106
http://dx.doi.org/10.1016/j.jallcom.2006.05.054

Figure 2

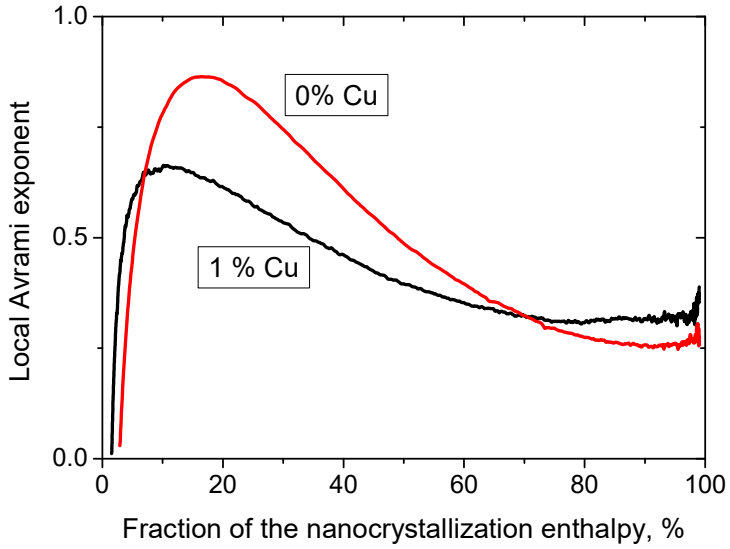

Journal of Alloys and Compounds. Vol. 431. Núm. 1-2. 2007. Pag. 100-106
http://dx.doi.org/10.1016/j.jallcom.2006.05.054

Figure 3

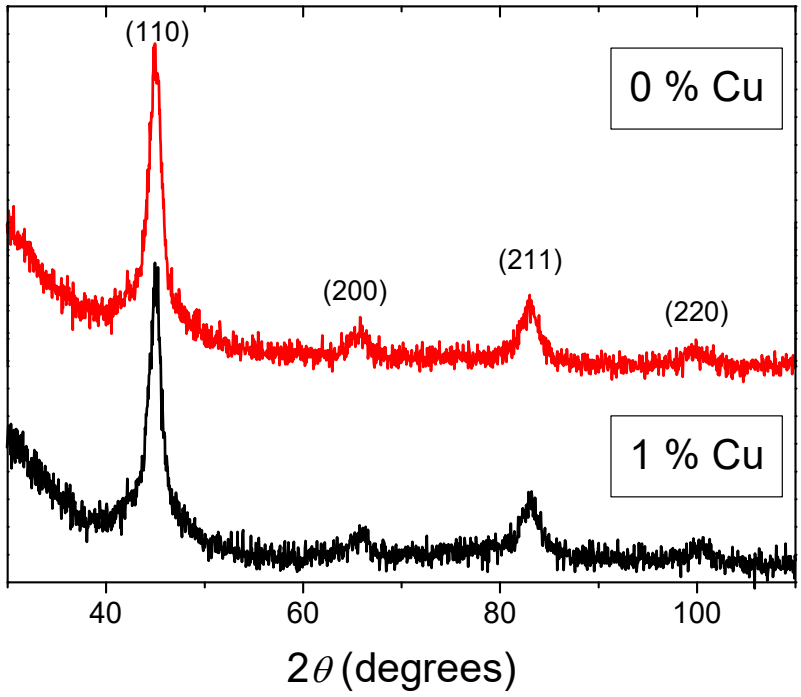

Journal of Alloys and Compounds. Vol. 431. Núm. 1-2. 2007. Pag. 100-106
http://dx.doi.org/10.1016/j.jallcom.2006.05.054

Figure 4

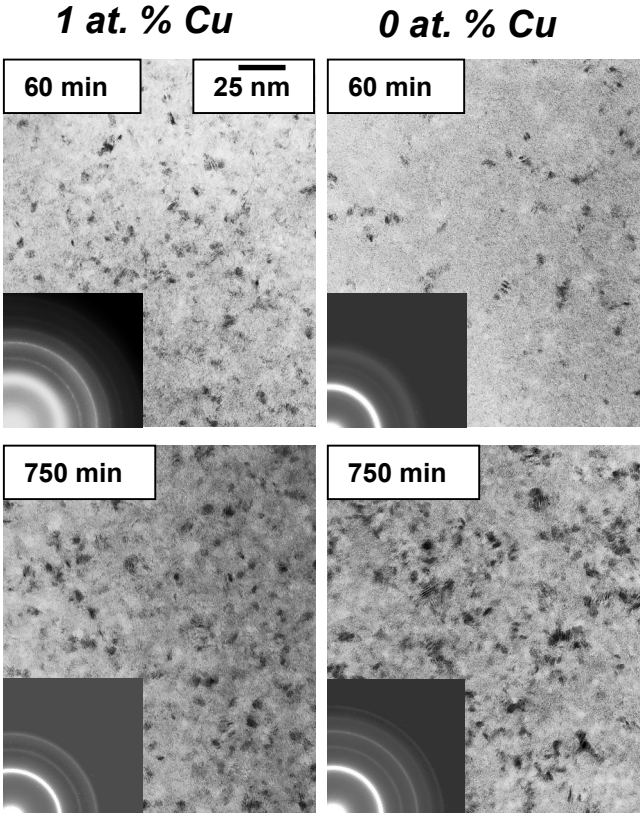

Journal of Alloys and Compounds. Vol. 431. Núm. 1-2. 2007. Pag. 100-106
http://dx.doi.org/10.1016/j.jallcom.2006.05.054

Figure 5

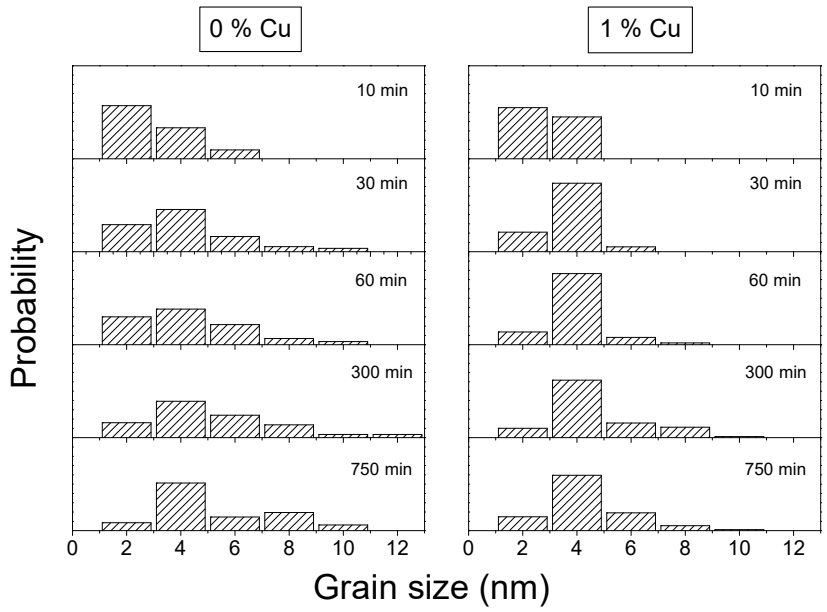

Journal of Alloys and Compounds. Vol. 431. Núm. 1-2. 2007. Pag. 100-106
http://dx.doi.org/10.1016/j.jallcom.2006.05.054

Figure 6

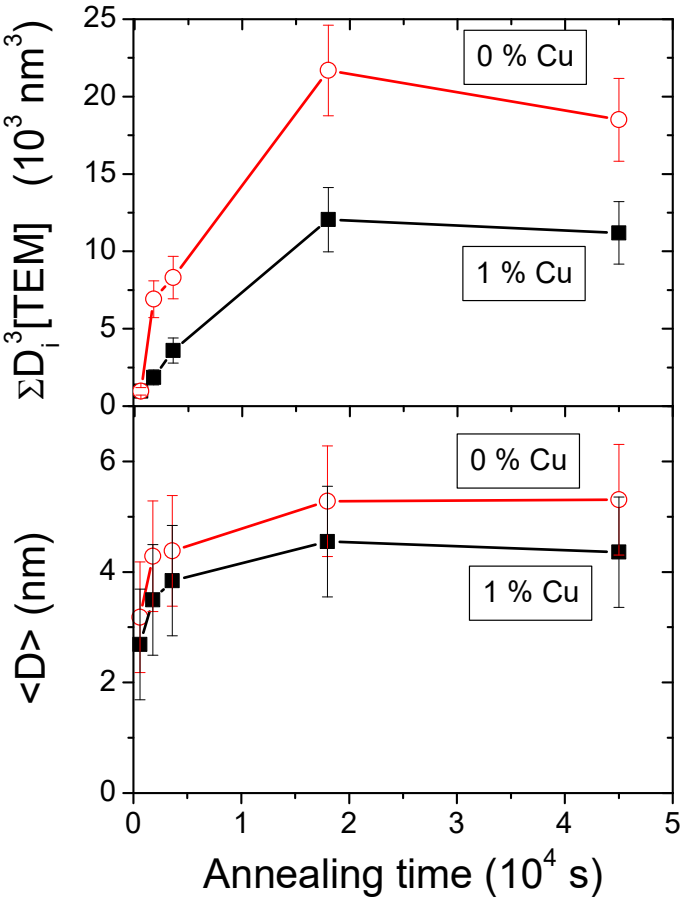

Journal of Alloys and Compounds. Vol. 431. Núm. 1-2. 2007. Pag. 100-106
http://dx.doi.org/10.1016/j.jallcom.2006.05.054

Figure 7

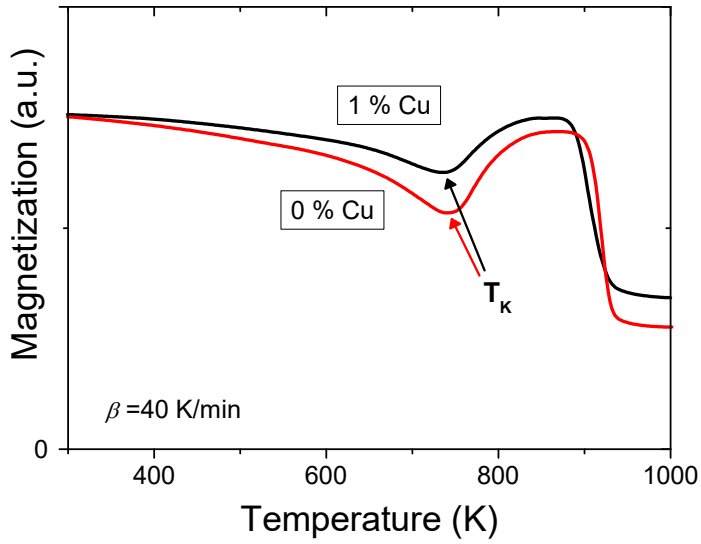

Journal of Alloys and Compounds. Vol. 431. Núm. 1-2. 2007. Pag. 100-106
http://dx.doi.org/10.1016/j.jallcom.2006.05.054

Figure 8

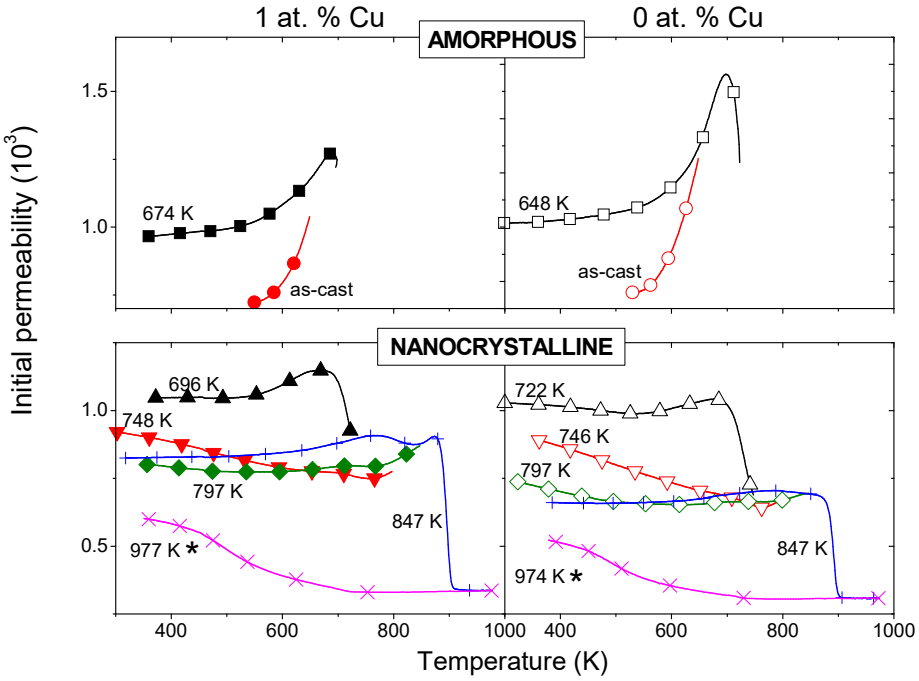

Journal of Alloys and Compounds. Vol. 431. Núm. 1-2. 2007. Pag. 100-106
http://dx.doi.org/10.1016/j.jallcom.2006.05.054

Figure 9